Low seismic resolution cannot explain S/P decorrelation in the lower mantle

S. Della Mora,[1] L. Boschi,[1] P. J. Tackley,[1] T. Nakagawa,[1] and D. Giardini[1]

Received 25 March 2011; revised 16 May 2011; accepted 18 May 2011; published 29 June 2011.

[1] Inverted models of the deep mantle show a decorrelation between maps of shear V_S and compressional V_P wave velocities, an anti-correlation between the bulk sound velocity V_ϕ and V_S and a much larger variability of V_S with respect to V_P, expressed by large values of the ratio of their relative lateral variations. We carried out synthetic tests to verify if these features could be artifacts, explained by limits in tomographic resolution: synthetic data are calculated for an "input" model, and linearly inverted, as in tomography, to find an "output" model. Comparing the values of the aforementioned parameters for two different chemically homogeneous input models with the associated reconstructed output ones, we found that artifacts caused by realistic data noise and the nonuniform distribution of seismic sources and stations over the globe are not sufficient to introduce the features previously described. We confirm that compositional effects are required to explain them. **Citation:** Della Mora, S., L. Boschi, P. J. Tackley, T. Nakagawa, and D. Giardini (2011), Low seismic resolution cannot explain S/P decorrelation in the lower mantle, *Geophys. Res. Lett.*, *38*, L12303, doi:10.1029/2011GL047559.

1. Introduction

[2] There are a few solid results about the nature of heterogeneities in the deep mantle:

[3] 1. The correlation

$$r_{P,S} = \frac{\sum_{i=1}^{N}\left[\delta(\ln V_P)_i - \overline{\delta(\ln V_P)}\right]\left[\delta(\ln V_S)_i - \overline{\delta(\ln V_S)}\right]}{\left[\left(\sum_{i=1}^{N}\left[\delta(\ln V_P)_i - \overline{\delta(\ln V_P)}\right]^2\right)\left(\sum_{i=1}^{N}\left[\delta(\ln V_S)_i - \overline{\delta(\ln V_S)}\right]^2\right)\right]^{\frac{1}{2}}} \quad (1)$$

between compressional (V_P) and shear (V_S) wave relative velocity anomalies (δ ($\ln V_P$) and δ ($\ln V_S$), respectively) at a certain depth (the quantities with a bar are the averages at the considered depth), is fairly high throughout the mantle but drops in the lowermost mantle [*Saltzer et al.*, 2001; *Becker and Boschi*, 2002; *Ishii and Tromp*, 2004; *Simmons et al.*, 2010].

[4] 2. $r_{\phi,S}$ between bulk sound (V_ϕ) and V_S relative anomalies (δ ($\ln V_\phi$) and δ ($\ln V_S$), respectively) at a certain depth (found replacing V_P with V_ϕ in equation (1)) is negative in the lowermost mantle [*Su and Dziewonski*, 1997; *Antolik et al.*, 2003; *Kennett and Gorbatov*, 2004; *Hutko et al.*, 2008].

[5] 3. The ratio

$$R_{S,P} = \sum_{i=1}^{N} \frac{\delta(\ln V_S)_i - \overline{\delta(\ln V_S)}}{\delta(\ln V_P)_i - \overline{\delta(\ln V_P)}} \quad (2)$$

is high in the lowermost mantle ($R_{S,P} > 2.5$), indicating larger V_S than V_P variability [*Robertson and Woodhouse*, 1996; *Masters et al.*, 2000; *Karato and Karki*, 2001; *Ritsema and Van Heijst*, 2002].

[6] In a chemically homogeneous mantle, where seismic heterogeneity is caused by thermal anomalies alone, we expect $R_{S,P} < 2.5$ [*Karato*, 2003] and high $r_{P,S}$ and $r_{\phi,S}$ [*Hirose*, 2006]. The aforementioned results indicate that chemical composition has an influence on seismic heterogeneity, at least in the lowermost mantle.

[7] It has nonetheless been suggested by *Schuberth et al.* [2009] that "isochemical whole-mantle flow with strong core heating and a pyrolite composition can be reconciled with tomography". This is in contrast with the statement by *Ritsema et al.* [2007] that "Temperature anomalies in the thermochemical model resemble the spatial extent of low seismic velocity anomalies and the shear velocity spectrum in the D'' region better than the isochemical model."

[8] Both *Ritsema et al.* [2007] and *Schuberth et al.* [2009] evaluate tomographic resolution of *S*-wave travel-time data only. We extend their treatment to *P*-wave tomography to determine if low resolution of seismic tomography can explain inconsistencies from an isochemical model. We apply the tomography resolution operator associated with common *P* and *S* travel-time coverage to isochemical mantle models, and verify whether or not values of $r_{P,S}$, $r_{\phi,S}$ and $R_{S,P}$ found from the data can be explained as artifacts of low tomographic resolution.

2. *S*- and *P*-Travel-Time Tomography

[9] We invert body-wave travel-time delays in the regularized least-squares framework of *Boschi and Dziewonski* [1999]. In both *P*- and *S*-wave inversions, we consistently select the solution from the "corner-region" of the L-curve [*Hansen*, 1992], while checking its general consistency with other recent mantle tomography results [e.g., *Boschi et al.*, 2007, 2008].

[10] The inverted model is parameterized with 5° size blocks horizontally and 29 layers vertically. We employ ≈620,000 direct *P*-wave arrivals based on the ISC bulletin with sources relocated by *Antolik et al.* [2003] and ≈170,000 *S*-wave ones measured via cross-correlation by *Houser et al.* [2008]. The data were corrected for crustal structure by the authors. *S*-wave arrivals are much fewer than *P*-wave ones because of the inherent difficulty of making an *S*-wave travel-time pick with respect to a *P*-wave one.

[1]Institute of Geophysics, ETH Zurich, Zurich, Switzerland.

0094-8276/11/2011GL047559

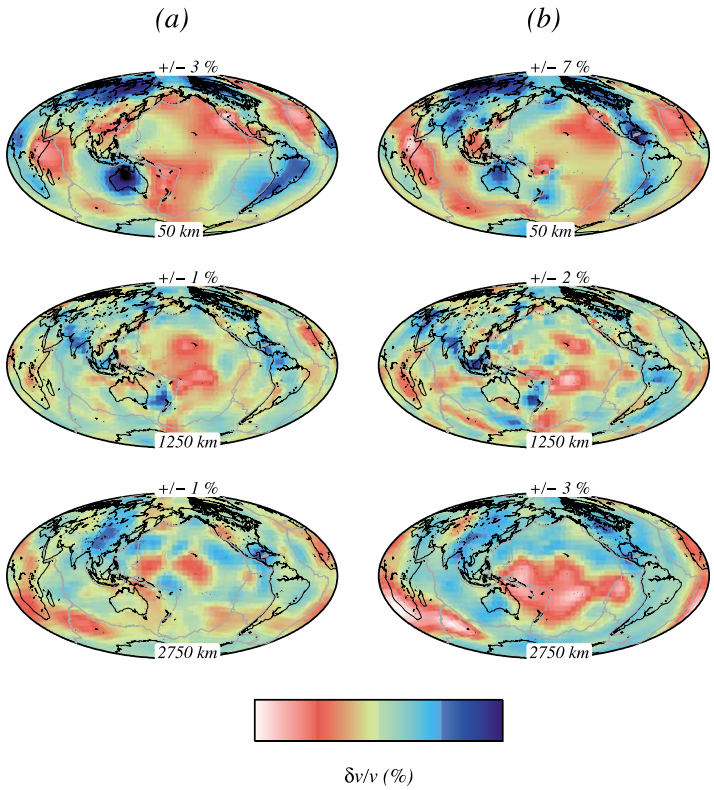

Figure 1. (a) V_P tomography map from the direct P arrivals dataset of *Antolik et al.* [2003]. (b) V_S tomography from direct S arrivals of *Houser et al.* [2008]. On each panel, the range of plotted values and the depth of the plotted layer are given.

[11] The results of the inversions are shown in Figure 1. The main subduction zones and cratonic regions are visible in both V_P (Figure 1a) and V_S (Figure 1b). A smaller variability is observed in the mid-mantle. In the lowermost mantle, the two large low-velocity provinces under Africa and the Pacific are reproduced in both V_S and, to some extent, V_P [e.g., *Wang and Wen*, 2004; *Hernlund and Houser*, 2008].

[12] We calculate V_ϕ and δ ($\ln V_\phi$) based on equations (1) and (2) of *Masters et al.* [2000], and then find $r_{\phi,S}$, $r_{P,S}$ and

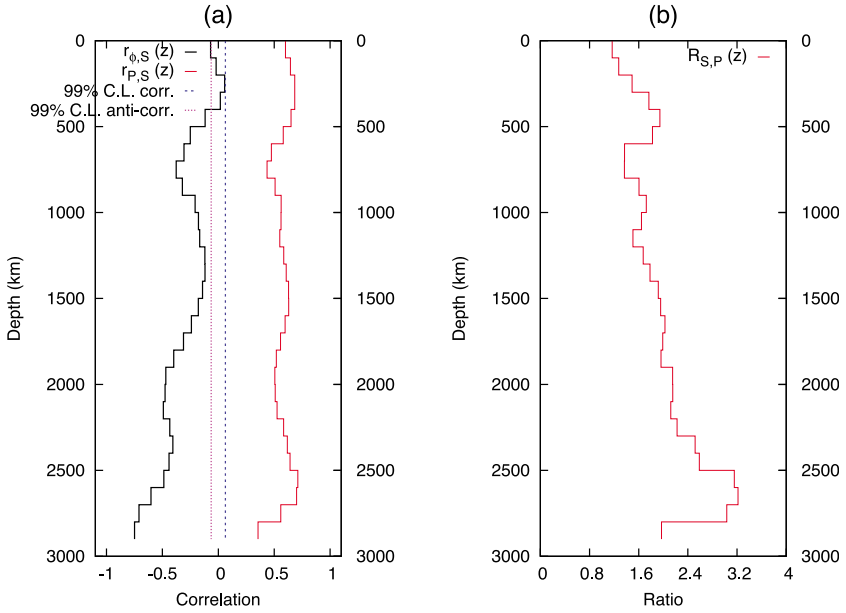

Figure 2. (a) Correlations $r_{\phi,S}$ (black solid curve) and $r_{P,S}$ (red solid) as a function of depth from the models of Figure 1, compared with the level of 99% significance of correlation (blue dashed curve) and anti-correlation (purple dashed). (b) The ratio $R_{S,P}$ from the models of Figure 1.

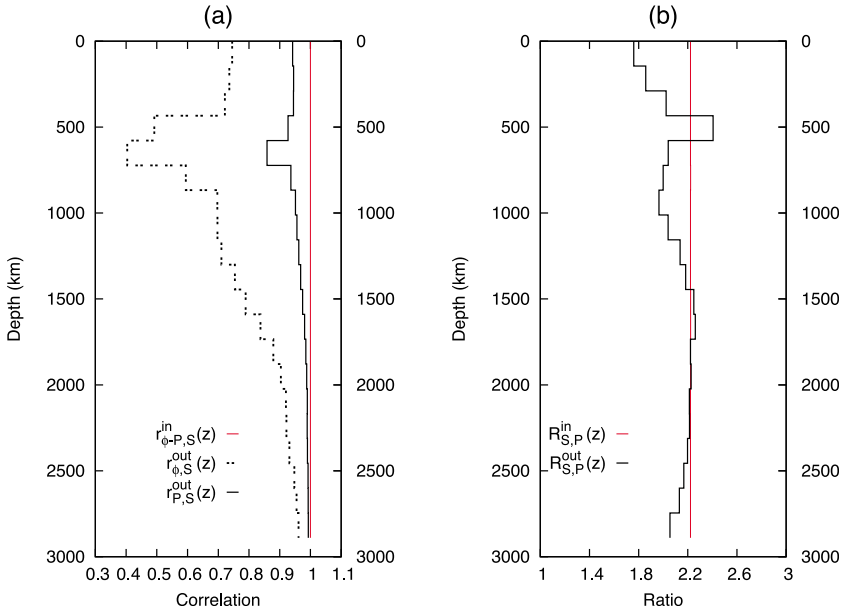

Figure 3. (a) $r^{in}_{\phi,S}$ and $r^{in}_{P,S}$ (red solid curve) for the model 045S-SMEAN, and $r^{out}_{\phi,S}$ (black dashed curve) and $r^{out}_{P,S}$ (black solid curve) for the model reconstructed by tomography. (b) $R^{in}_{S,P}$ for 045S-SMEAN (red curve) and $R^{out}_{S,P}$ for the reconstructed model (black).

$R_{S,P}$ as functions of depth as defined in Section 1. In the calculation of $R_{S,P}$ we discard the points in which either $|\delta(\ln V_S) - \overline{\delta(\ln V_S)}| < 0.2\%$ or $|\delta(\ln V_P)_i - \overline{\delta(\ln V_P)}| < 0.2\%$. This way and with the definition of equation (2) we remove the arbitrariness of the reference model choice and the values that cannot be distinguished from numerical noise.

[13] Figure 2 shows $r_{\phi,S}$, $r_{P,S}$ and $R_{S,P}$ from the tomographic maps of Figure 1. $r_{P,S}$ is significantly positive throughout the mantle, but, consistently with Figure 10 of *Becker and Boschi* [2002], it decreases in the bottom 300 km, where the phase transition from perovskite to post-perovskite is thought to occur [e.g., *Oganov and Ono*, 2004]. In the mid- and deep mantle $r_{\phi,S}$ is always significantly negative, with a noticeable decrease between 1500 and 2000 km and the last 300 km of mantle. If we compare this result, e.g., with Figure 9 of *Antolik et al.* [2003], we notice that for both the value of the correlation in the mid-mantle is ≈−0.5, but in Figure 2 it decreases in the lowermost mantle, whereas the correlation of *Antolik et al.* [2003] does not vary with respect to the above layers. The values of $R_{S,P}$ in the lowermost mantle are > 2.5, indicating a larger lateral variability of V_S with respect to V_P. From *Karato* [2003], as already reminded in Section 1, we know that values $R_{S,P} > 2.5$ cannot be explained by a chemically homogeneous mantle circulation model. We then conclude that, at least in the last 300 km of mantle, all these results are an indication of the importance of compositional effects [e.g., *Karato and Karki*, 2001]. We are skeptical about the sudden decrease of $r_{P,S}$ and $R_{S,P}$ right above the core-mantle boundary (CMB): our datasets only include direct phases, and, in the absence of core-reflected/refracted ones, resolution will tend to drop at the very bottom of the mantle, so that this effect could be an artifact.

3. Synthetic Experiments

[14] The results summarized in Section 2 point to the existence of compositional heterogeneities. Yet, it is a priori possible that the decorrelation and high ratio between $\delta(\ln V_S)$ and $\delta(\ln V_P)$ can be caused by the uneven lateral and radial coverage of the seismic datasets, and to the differences in sampling between *S*- and *P*-waves. $\delta(\ln V_P)$ and $\delta(\ln V_S)$ are well resolved over different volumes of the mantle, which will systematically lower the correlation of their tomographic images. The tomography resolution operator **R** shows how real Earth properties are mapped into a tomographic model [e.g., *Boschi*, 2003; *Ritsema et al.*, 2007; *Bull et al.*, 2010]. To verify if resolution has significant effects on the measurements of $r_{P,S}$, $r_{\phi,S}$ and $R_{S,P}$, we generate synthetic travel-time delays from a known input model, making use of the same stations and sources of *Antolik et al.* [2003] and *Houser et al.* [2008]. We follow the ray-theory approximation on a 1-D reference model, resulting in a linear relation between model anomalies and data. Details are given by, e.g., *Boschi and Dziewonski* [1999]. The generated data include Gaussian noise with a standard deviation of 1 s for P waves and 3 s for S waves. We invert those data with the same procedure employed in Section 2 and the same regularization parameters of the solutions shown in Figure 1, calculate the correlations $r_{P,S}$ and $r_{\phi,S}$ and the ratio $R_{S,P}$ for both the input and the reconstructed model and compare them to evaluate the effects of tomographic resolution. This is equivalent, given an input model **m**, to comparing **m** and **R** · **m**. *Schuberth et al.* [2009] conducted a similar experiment, but limited their analysis to *S*-wave tomography. We repeat this procedure for two models that reproduce the behavior of an isochemical mantle:

[15] 1. The first model has the V_S distribution of SMEAN of *Becker and Boschi* [2002], while the V_P anomalies are simply obtained by multiplying the values of V_S anomalies by of 0.45 (hereafter, this model will be denoted as 045S-SMEAN), based on the results from Figure 2 of *Karato* [1993]. The model has $r^{in}_{\phi,S} = r^{in}_{P,S} = 1$ and $R^{in}_{S,P} = 2.22$ constant at all layers (Figure 3).

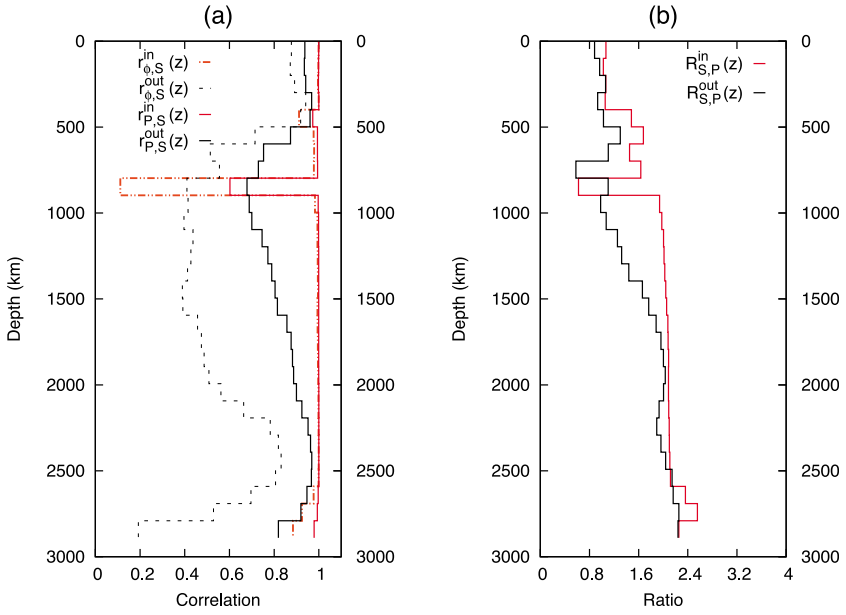

Figure 4. Same as Figure 3, but for the input isochemical mantle circulation model of *Nakagawa et al.* [2009].

[16] 2. The second one is a purely thermal mantle circulation model, whose details are given by *Nakagawa et al.* [2009]. This model has material properties calculated using a self-consistent mineralogical treatment based on minimization of free energy, i.e., the scaling between temperature and (V_S,V_P) is not a-priori linear. From Figure 4 one can see that, as expected, both the input correlations $r^{in}_{\phi,S}$ and $r^{in}_{P,S}$ are very close to 1, except right below the region where the phase transition from ringwoodite to perovskite and magnesiowüstite occurs [*Ono and Oganov*, 2005].

3.1. Resolution of Model 045S-SMEAN

[17] We compare in Figure 3 the values of $r_{\phi,S}$, $r_{P,S}$ and $R_{S,P}$ associated with model 045S-SMEAN, with those found from the inversion of 045S-SMEAN-generated data.

[18] The correlation $r^{out}_{\phi,S}$ for the reconstructed model changes significantly in the upper mantle, where our database, that contains only direct body waves, has very limited resolution [*Boschi*, 2003]. In the lower mantle, from a depth of about 1800 km, the correlation is 0.97, indicating that limits in tomography resolution do not significantly deteriorate the complete correlation between V_ϕ and V_S variations; $r^{out}_{P,S}$ is even less perturbed with respect to $r^{in}_{P,S} = 1$. This happens because V_ϕ is a function of V_P and V_S, so the uncertainties on V_ϕ are larger than those on V_P or V_S. We observe a similar behavior for the ratio $R_{S,P}$, which is almost the same for the input (red curve) and the output (black curve) model between 1500 and 2500 km depth. There is a slight decrease of $R^{out}_{S,P}$ right at the CMB, owing probably to the data-coverage problems mentioned in Section 2.

3.2. Resolution of a Geodynamical Isochemical Model

[19] The model of the previous section is unrealistic, since it does not include phase transitions that can still occur in a purely thermal model. We therefore generate and invert a synthetic dataset based on a geodynamical model by *Nakagawa et al.* [2009].

[20] The results (Figure 4) are similar to those of Section 3.1. Both the correlations in the output model $r^{out}_{\phi,S}$ and $r^{out}_{P,S}$ are always significant with a confidence level higher than 99% and similar to the associated input $r^{in}_{\phi,S}$ and $r^{in}_{P,S}$, but we cannot reconstruct the sudden decrease of correlation at 850 km of the input model mentioned in Section 3. In the bottom mantle layer both $r^{out}_{P,S}$ and $r^{out}_{\phi,S}$ decrease, but, as mentioned, resolution within this layer is low. The comparison between $R^{in}_{S,P}$ and $R^{out}_{S,P}$ is good from 1600 km depth down, the region where the datasets of direct arrivals that we employed have higher resolution [*Boschi*, 2003].

4. Discussion and Conclusions

[21] We have inverted *P*- and *S*-wave travel-times as illustrated in Figure 2 and discussed in Section 2.

[22] We confirm a significant anti-correlation between V_ϕ and V_S, with a relevant decrease of $r_{\phi,S}$ between 2500 km and the CMB. Correlation $r_{P,S}$ is high at all mantle depths, except for the bottom 100 km. The ratio $R_{S,P}$ also drops in our lowermost mantle layer, but is very large (i.e., >2.5) between 2500 and 2800 km depth, with a sharp change from $R_{S,P} \approx 2.5$ to $R_{S,P} \approx 3.0$ at 2500 km. The very bottom layer (2800–2900 km) in our parameterization is only sampled by the small subsets of *P* and *S* travel-times whose associated ray paths bottom in this depth range, with inherent resolution problems; we do not attribute much significance to the bottom layer, but consider our results robust over the rest of the lower mantle. The upper mantle is also notoriously undersampled by body waves [e.g., *Boschi and Dziewonski*, 1999].

[23] Our results are first of all consistent with studies that indicate the presence of a compositional signature on deep-mantle seismic velocities. For example, *Cammarano et al.* [2003] show the importance of compositional effects on the ratio $R_{S,P}$ through the whole mantle. *Tsuchiya et al.* [2004] give an alternative explanation, showing from first principle calculations that post-perovskite, likely the most abundant phase in the *D″*, has larger V_S than V_ϕ variations.

From similar ab initio calculations *Wookey et al.* [2005] obtained for post-perovskite values of $r_{\phi,S} < 0$.

[24] Secondly, other seismic studies have also shown the importance of compositional effects in the deep mantle. For instance, *Trampert et al.* [2004] employed probabilistic tomography to highlight the importance of compositional effects on seismic velocities in the lower mantle. More recently, *Hernlund and Houser* [2008] have compared different tomographic models and showed that the distributions of V_P and V_S are uncoupled in the deep mantle. Similarly, *Boschi et al.* [2007, 2008] show that presumed lowermost mantle plumes have a different signature in *P*- vs. *S*-velocity tomography.

[25] Last, results in geodynamical models have shown the importance of compositional effects. For example, *Tan and Gurnis* [2007] have shown the effects on seismic velocities of a chemical layer at the base of the mantle and its possible evolution in time. *Tackley* [2008] indicated that a mixed thermo-chemical mantle model is probably closest to the true Earth's mantle model. *Nakagawa et al.* [2010] have evidenced the importance of small variations in MORB composition on mantle circulation.

[26] In Section 3, we addressed the question of whether the existence of compositional heterogeneity in the mantle, as it is currently inferred from tomography, can be interpreted as an artifact caused by low seismic resolution. To solve this problem, we performed two synthetic resolution tests with input models that reproduce the seismic characteristics of a purely thermal mantle circulation.

[27] We first tested how our data resolve a model with perfect correlation between lateral V_P and V_S variations, and found that from 1500 km down this property is essentially reproduced by the reconstructed model. Additionally, the input model had $R^{in}_{S,P} = 2.2$ constant for all the layers, and this essentially holds for the output model from 1500 km down.

[28] We conducted an analogous test, inverting a synthetic dataset generated from the seismic velocity structure associated with the isochemical geodynamical model of *Nakagawa et al.* [2009]. The input model had both $r^{in}_{\phi,S} = r^{in}_{P,S} = 1$, except for the 800–900 km layer. In the reconstructed model this feature is smeared over a wide depth-range, but, besides this effect, the correlation is always significantly positive. From 1800 km down, the values of $R_{S,P}$ for the input and output model are very similar, indicating again that the dataset that we generated has enough resolution in this depth-range.

[29] These tests confirm that seismic resolution of lower mantle is sufficient to constrain $r_{\phi,S}$, $r_{P,S}$ and $R_{S,P}$ consistently.

[30] **Acknowledgments.** Fabio Cammarano contributed to this work with many insightful comments. We thank Christine Houser for sharing her S-travel-time database.

[31] The Editor thanks Mark Panning and an anonymous reviewer for their assistance in evaluating this paper.

References

Antolik, M., Y. J. Gu, G. Ekström, and A. M. Dziewonski (2003), J362D28: A new joint model of compressional and shear velocity in the Earth's mantle, *Geophys. J. Int.*, *153*(2), 443–466, doi:10.1046/j.1365-246X.2003.01910.x.

Becker, T., and L. Boschi (2002), A comparison of tomographic and geodynamic mantle models, *Geochem. Geophys. Geosyst.*, *3*(1), 1003, doi:10.1029/2001GC000168.

Boschi, L. (2003), Measures of resolution in global body wave tomography, *Geophys. Res. Lett.*, *30*(19), 1978, doi:10.1029/2003GL018222.

Boschi, L., and A. M. Dziewonski (1999), High- and low-resolution images of the Earth's mantle: Implications of different approaches to tomographic modeling, *J. Geophys. Res.*, *104*(B11), 25,567–25,594, doi:10.1029/1999JB900166.

Boschi, L., T. W. Becker, and B. Steinberger (2007), Mantle plumes: Dynamic models and seismic images, *Geochem. Geophys. Geosyst.*, *8*, Q10006, doi:10.1029/2007GC001733.

Boschi, L., T. W. Becker, and B. Steinberger (2008), On the statistical significance of correlations between synthetic mantle plumes and tomographic models, *Phys. Earth Planet. Inter.*, *167*(3–4), 230–238, doi:10.1016/j.pepi.2008.03.009.

Bull, A. L., A. K. McNamara, T. W. Becker, and J. Ritsema (2010), Global scale models of the mantle flow field predicted by synthetic tomography models, *Phys. Earth Planet. Inter.*, *182*(3–4), 129–138, doi:10.1016/j.pepi.2010.03.004.

Cammarano, F., S. Goes, P. Vacher, and D. Giardini (2003), Inferring upper-mantle temperatures from seismic velocities, *Phys. Earth Planet. Inter.*, *138*(3–4), 197–222, doi:10.1016/S0031-9201(03)00156-0.

Hansen, P. C. (1992), Analysis of discrete ill-posed problems by means of the L-curve, *SIAM Rev.*, *34*(4), 561–580.

Hernlund, J. W., and C. Houser (2008), On the statistical distribution of seismic velocities in Earth's deep mantle, *Earth Planet. Sci. Lett.*, *265*(3–4), 423–437, doi:10.1016/j.epsl.2007.10.042.

Hirose, K. (2006), Postperovskite phase transition and its geophysical implications, *Rev. Geophys.*, *44*, RG3001, doi:10.1029/2005RG000186.

Houser, C., G. Masters, P. Shearer, and G. Laske (2008), Shear and compressional velocity models of the mantle from cluster analysis of long-period waveforms, *Geophys. J. Int.*, *174*(1), 195–212, doi:10.1111/j.1365-246X.2008.03763.x.

Hutko, A. R., T. Lay, J. Revenaugh, and E. J. Garnero (2008), Anticorrelated seismic velocity anomalies from post-perovskite in the lowermost mantle, *Science*, *320*(5879), 1070–1074, doi:10.1126/science.1155822.

Ishii, M., and J. Tromp (2004), Constraining large-scale mantle heterogeneity using mantle and inner-core sensitive normal modes, *Phys. Earth Planet. Inter.*, *146*(1–2), 113–124, doi:10.1016/j.pepi.2003.06.012.

Karato, S. (1993), Importance of anelasticity in the interpretation of seismic tomography, *Geophys. Res. Lett.*, *20*(15), 1623–1626, doi:10.1029/93GL01767.

Karato, S.-I. (2003), *The Dynamic Structure of the Deep Earth: An Interdisciplinary Approach*, 241 pp., Princeton Univ. Press, Princeton, N. J.

Karato, S., and B. B. Karki (2001), Origin of lateral variation of seismic wave velocities and density in the deep mantle, *J. Geophys. Res.*, *106*, 21,771–21,783, doi:10.1029/2001JB000214.

Kennett, B. L. N., and A. Gorbatov (2004), Seismic heterogeneity in the mantle—Strong shear wave signature of slabs from joint tomography, *Phys. Earth Planet. Inter.*, *146*(1–2), 87–100, doi:10.1016/j.pepi.2003.07.033.

Masters, G., G. Laske, H. Bolton, and A. Dziewonski (2000), The relative behavior of shear velocity, bulk sound speed, and compressional velocity in the mantle: Implications for chemical and thermal structure, in *Earth's Deep Interior: Mineral Physics and Tomography from the Atomic to the Global Scale*, *Geophys. Monogr. Ser.*, vol. 117, edited by S.-I. Karato et al., pp. 63–87, AGU, Washington, D. C.

Nakagawa, T., P. J. Tackley, F. Deschamps, and J. A. D. Connolly (2009), Incorporating self-consistently calculated mineral physics into thermo-chemical mantle convection simulations in a 3-D spherical shell and its influence on seismic anomalies in Earth's mantle, *Geochem. Geophys. Geosyst.*, *10*, Q03004, doi:10.1029/2008GC002280.

Nakagawa, T., P. Tackley, F. Deschamps, and J. A. D. Connolly (2010), The influence of morb and harzburgite composition on thermo-chemical mantle convection in a 3-D spherical shell with self-consistently calculated mineral physics, *Earth Planet. Sci. Lett.*, *296*(3–4), 403–412, doi:10.1016/j.epsl.2010.05.026.

Oganov, A. R., and S. Ono (2004), Theoretical and experimental evidence for a post-perovskite phase of $MgSiO_3$ in Earth's D″ layer, *Nature*, *430*, 445–448, doi:10.1038/nature02701.

Ono, S., and A. Oganov (2005), In situ observations of phase transition between perovskite and $CaIrO_3$-type phase in $MgSiO_3$ and pyrolitic mantle composition, *Earth Planet. Sci. Lett.*, *236*(3–4), 914–932, doi:10.1016/j.epsl.2005.06.001.

Ritsema, J., and H.-J. Van Heijst (2002), Constraints on the correlation of *P*- and *S*-wave velocity heterogeneity in the mantle from *P*, *PP*, *PPP* and *PKP*ab traveltimes, *Geophys. J. Int.*, *149*(2), 482–489, doi:10.1046/j.1365-246X.2002.01631.x.

Ritsema, J., A. K. McNamara, and A. L. Bull (2007), Tomographic filtering of geodynamic models: Implications for model interpretation and large-scale mantle structure, *J. Geophys. Res.*, *112*, B01303, doi:10.1029/2006JB004566.

Robertson, G., and J. Woodhouse (1996), Ratio of relative *S* to *P* velocity heterogeneity in the lower mantle, *J. Geophys. Res.*, *101*(B9), 20,041–20,052.

Saltzer, R. L., R. D. van der Hilst, and H. Kárason (2001), Comparing *P* and *S* wave heterogeneity in the mantle, *Geophys. Res. Lett.*, *28*(7), 1335–1338, doi:10.1029/2000GL012339.

Schuberth, B. S. A., H.-P. Bunge, and J. Ritsema (2009), Tomographic filtering of high-resolution mantle circulation models: Can seismic heterogeneity be explained by temperature alone?, *Geochem. Geophys. Geosyst.*, *10*, Q05W03, doi:10.1029/2009GC002401.

Simmons, N. A., A. M. Forte, L. Boschi, and S. P. Grand (2010), GyPSuM: A joint tomographic model of mantle density and seismic wave speeds, *J. Geophys. Res.*, *115*, B12310, doi:10.1029/2010JB007631.

Su, W.-J., and A. M. Dziewonski (1997), Simultaneous inversion for 3-D variations in shear and bulk velocity in the mantle, *Phys. Earth Planet. Inter.*, *100*(1–4), 135–156, doi:10.1016/S0031-9201(96)03236-0.

Tackley, P. J. (2008), Layer cake or plum pudding?, *Nat. Geosci.*, *1*(3), 157–158, doi:10.1038/ngeo134.

Tan, E. and M. Gurnis (2007), Compressible thermochemical convection and application to lower mantle structures, *J. Geophys. Res.*, *112*, B06304, doi:10.1029/2006JB004505.

Trampert, J., F. Deschamps, J. Resovsky, and D. Yuen (2004), Probabilistic tomography maps chemical heterogeneities throughout the lower mantle, *Science*, *29*, 853–856, doi:10.1126/science.1101996.

Tsuchiya, T., J. Tsuchiya, K. Umemoto, and R. M. Wentzcovitch (2004), Elasticity of post-perovskite $MgSiO_3$, *Geophys. Res. Lett.*, *31*, L14603, doi:10.1029/2004GL020278.

Wang, Y., and L. Wen (2004), Mapping the geometry and geographic distribution of a very low velocity province at the base of the Earth's mantle, *J. Geophys. Res.*, *109*, B10305, doi:10.1029/2003JB002674.

Wookey, J., S. Stackhouse, J. M. Kendall, J. Brodholt, and G. D. Price (2005), Efficacy of the post-perovskite phase as an explanation for lowermost-mantle seismic properties, *Nature*, *438*, 1004–1007, doi:10.1038/nature04345.

L. Boschi, S. Della Mora, D. Giardini, T. Nakagawa, and P. J. Tackley, Institute of Geophysics, ETH Zurich, Sonnesggstrasse 5, CH-8092 Zurich, Switzerland. (dellamora@tomo.ig.erdw.ethz.ch)